Spin-wave method for the total energy of paramagnetic state

A. V. Ruban* and V. I. Razumovskiy
Department of Materials Science and Engineering, KTH Royal Institute of Technology, SE-100 44 Stockholm, Sweden
(Received 17 February 2012; published 7 May 2012)

Spin-wave formalism provides a convenient alternative way of modeling the high-temperature paramagnetic state for a certain type of magnets within the framework of Hamiltonian-type electronic-structure methods. For Heisenberg systems, it is formally equivalent to the so-called disordered local moment approach, which is usually used in the methods based on the coherent potential approximation within the Green's function or multiple-scattering techniques. In this paper, we demonstrate that the spin-wave method has certain advantages when it comes to the calculation of forces and relaxations. It also allows one to take magnetic short-range-order effects into consideration. As examples of the application of the spin-wave method, we calculate the energy of the paramagnetic state in fcc Co and bcc Fe, the vacancy formation energy, elastic constants, and phonon spectrum in bcc paramagnetic Fe. We demonstrate that magnetic short-range-order effects play a crucial role in the mechanical stabilization of the bcc Fe at high temperature in the paramagnetic state.

DOI: 10.1103/PhysRevB.85.174407 PACS number(s): 75.10.−b, 75.50.Bb, 75.30.Ds

I. INTRODUCTION

Accurate first-principles modeling of magnetic systems at high temperatures in the paramagnetic (PM) state requires methods going beyond the standard density functional theory (DFT), which can take all the possible magnetic excitations into consideration, such as, for instance, a dynamic mean field theory (DMFT).[1] However, in cases when transverse magnetic fluctuations are dominant, the use of a simple so-called disordered local moment model[2–5] (DLM) provides a reasonable description of the electronic structure and energetics of paramagnetic state. In this model, the paramagnetic state is given by a random orientation of the spin magnetic moments on different atoms, which is the case when transverse fluctuations of the local magnetic moment occur on time scales less than the typical time of electron hopping between atoms.

As has been demonstrated by Gyorffy *et al.*,[5] in the absence of the spin-orbit interaction (scalar-relativistic case), DLM is equivalent to the collinear system with randomly distributed spin-up and spin-down local magnetic moments. This allows one to use a very efficient and quite accurate in this particular case coherent potential approximation[6,7] (CPA) in order to obtain the electronic structure and other related properties of the system in the paramagnetic state. With the advance of computational techniques and computers, the supercell modeling of random alloys has also become available, and it is also used nowadays for the modeling of the paramagnetic state.[8–10]

Both CPA and supercell approaches have their advantages and problems. In the case of the CPA, the main problem is a reduced accuracy of the corresponding DFT calculations, so the CPA-based methods, for instance, can be hardly used for calculating phonon spectrum, local lattice relaxations in random alloys in the DLM-paramagnetic state. At the same time, the supercell approach becomes cumbersome in the case of random alloys or large and inhomogeneous systems.

Another problem with the supercell approach is the fact that it can provide a DLM-like distribution of the magnetic moments only on average for the whole supercell, while specific local correlation functions are quite arbitrary. In this case, the modeling of local defects, such as vacancies, impurities, surfaces, interfaces, and so on, becomes quite time consuming due to the necessity to perform the corresponding configurational averaging *locally*.

One should also keep in mind that the random distribution of spins on the underlying lattice does not guarantee that the final result of the self-consistent calculations indeed corresponds to the DLM state since it applies only to the case where all the local magnetic moments have exactly the same magnitude, which is usually not the case for the systems with the itinerant type of magnetism.

In this paper, we suggest an alternative approach that can be used for calculations of the energetics of systems in paramagnetic state. It is based on spin-spiral calculations.[11,12] Let us note that the spin-spiral method has been previously used in calculations of the temperature-induced magnetic excitations in particular, including longitudinal spin fluctuations.[12–14] However, we will use the spin-spiral method just to model paramagnetic state. As we demonstrate in this paper, it yields reasonable description of the paramagnetic state in the case of bcc Fe, and can be used as an alternative to the usual supercell approach in the methods, which do not have the advantage of using the CPA.

II. FORMALISM

A. Ideal paramagnetic state within Heisenberg model

Let us assume that the magnetic energy of a system is accurately given by the classical Heisenberg Hamiltonian

$$H = -\sum_{p} \sum_{i,j \in p} J_p \mathbf{e}_i \mathbf{e}_j, \tag{1}$$

where J_p are the magnetic exchange interaction parameters for a given coordination shell p and $\mathbf{e}_i$ is the direction of the spin at site i. Magnetic configuration can be characterized by lattice spin-spin correlation functions ξ_p:

$$\xi_p \equiv \langle \mathbf{e}_i \mathbf{e}_j \rangle_p = \frac{1}{N} \sum_{i,j \in p} \mathbf{e}_i \mathbf{e}_j, \tag{2}$$

where N is the number of atoms in the system. The energy of a system having a specific magnetic configuration is

$-\sum_p J_p \xi_p$. Of course, in general one should consider higher-order interactions and correlation functions, but for simplicity we assume that only pair interactions are important. The "ideal" paramagnetic (IPM) state can be defined as the one with vanishing spin-spin correlation functions:

$$\xi_p = 0. \tag{3}$$

This implies that the energy of the paramagnetic state is exactly zero in this formalism, while, for instance, the energy of the ferromagnetic (FM) state is $E_{\mathrm{FM}} \equiv -J_0 = -\sum_p J_p$.

Since the magnetic interactions are constant in the Heisenberg model, the way condition (3) is satisfied does not matter. In the DLM model, for instance, the spin-spin correlation functions are equal to zero because on every coordination shell an atom with spin-up or -down magnetic moment has on average the same number of spin-up and -down neighbors. The electronic structure and total energy of such an alloy can be calculated either using the CPA or within *an appropriate* supercell approach.[15]

B. Spin-wave method for the total energy of the ideal paramagnetic state

Another way to satisfy condition (3) is to perform averaging over a proper set of magnetic systems. Every member of such a set can have an arbitrary magnetic structure, but their average should produce the needed result, i.e.,

$$\sum_i w_i \xi_{p;i} = 0 \tag{4}$$

for all relevant coordination shells p. Summation here runs over the set of magnetic systems having weights w_i and spin-spin correlation functions $\xi_{p;i}$. It is clear that the average energy of the set of the systems $\tilde{E} = \sum_p J_p \sum_i w_i \xi_{p;i} = 0$. In other words, the average of these energies produces exactly the energy of the paramagnetic state. The latter holds only in the case of Heisenberg systems, when magnetic exchange interactions J_p do not depend on the magnetic configuration.

A set, which satisfies this condition, is actually the set of the planar spin spirals (with the azimuth angle $\pi/2$) for all the wave vectors in the corresponding Brillouin zone (BZ). This is so since the spin-spin correlation function for two sites connected by vector $\mathbf{R}$ in the spin-spiral configuration with wave vector $\mathbf{q}$ is[11]

$$\xi_{\mathbf{q}}(\mathbf{R}) = \sin(\mathbf{qR}) + \cos(\mathbf{qR}), \tag{5}$$

and thus the superposition of all the spin spirals with different wave vectors $\mathbf{q}$:

$$\frac{1}{\Omega_{\mathrm{BZ}}} \int_{\mathrm{BZ}} d\mathbf{q}\, \xi_{\mathbf{q}}(\mathbf{R}) = \xi(\mathbf{R}) (\equiv \xi_{p,\mathbf{R}\in p}) = 0 \tag{6}$$

[except for $\mathbf{R} = 0$, since $\xi(\mathbf{R} = 0) = 1$], which is exactly the requirement for the correlation functions in the IPM.

Let us now determine the Fourier transform of the real-space correlation function

$$\xi(\mathbf{q}) = \frac{1}{2N} \sum_{\mathbf{R}} [\xi(\mathbf{R}) e^{i\mathbf{qR}} + \xi^*(\mathbf{R}) e^{-i\mathbf{qR}}], \tag{7}$$

from which the energy of the magnetic state with a specific choice of $\xi(\mathbf{q})$ is

$$E = \frac{1}{\Omega_{\mathrm{BZ}}} \int_{\mathrm{BZ}} d\mathbf{q}\, E(\mathbf{q}) \xi(\mathbf{q}), \tag{8}$$

where $E(\mathbf{q})$ is the energy of the planar spin spiral with wave vector $\mathbf{q}$.

It is clear that $\xi_q(\mathbf{q}')$, which corresponds to the planar spin spiral with $\xi(\mathbf{R})$ determined by Eq. (5), is the Dirac δ function $\xi_q(\mathbf{q}') = \delta(\mathbf{q} - \mathbf{q}')$, so that

$$E = \frac{1}{\Omega_{\mathrm{BZ}}} \int_{\mathrm{BZ}} d\mathbf{q}' E(\mathbf{q}') \xi_{\mathbf{q}}(\mathbf{q}') = E(\mathbf{q}). \tag{9}$$

The energy of the IPM state, which is given by the average over uniform distribution of planar spin spirals (6), can now be determined using Eq. (9):

$$\begin{aligned} E^{\mathrm{IPM}} &= \frac{1}{\Omega_{\mathrm{BZ}}^2} \int_{\mathrm{BZ}} d\mathbf{q} \int_{\mathrm{BZ}} d\mathbf{q}' E(\mathbf{q}') \xi_{\mathbf{q}}(\mathbf{q}') \\ &= \frac{1}{\Omega_{\mathrm{BZ}}} \int_{\mathrm{BZ}} d\mathbf{q}\, E(\mathbf{q}). \end{aligned} \tag{10}$$

Intuitively, Eq. (10) corresponds to the state when all the possible spin waves are fully excited. One should bear in mind that the above analysis is valid only for the case of planar spin spirals, although it can be easily generalized.

C. Special point technique

The potential advantage of the spin-wave approach is the possibility to use a very efficient special point technique[16–18] for the BZ integration. It was developed by Baldereschi[16] and Chadi and Cohen,[17] and a more general scheme was introduced by Monkhorst and Pack.[18] The integral over the Brillouin zone is reduced to the summation over a finite set of $\mathbf{q}$ points in the irreducible part of the BZ (IBZ), with weights determined by the multiplicity of the point in the BZ due to the point group of the reciprocal lattice. Since the number of points is finite, Eq. (6) does not hold anymore for arbitrary $\mathbf{R}$, and the average spin-spin correlation functions

$$\tilde{\xi}(\mathbf{R}) = \sum_i w_i \xi_{\mathbf{q}_i}(\mathbf{R}) \tag{11}$$

depend on the used set of $\mathbf{q}$ points.

In Tables I and II, we show $\tilde{\xi}(\mathbf{R})$ for the first 24 coordination shells in the fcc and bcc structures for different sets of $\mathbf{q}$ points. The first column represents the spin-spin correlation functions of the spin spirals for $\mathbf{q} = (0.6233, 0.2953, 0.0)$ and $\mathbf{q} = (\frac{1}{6}, \frac{1}{6}, \frac{1}{2})$ (in units $2\pi/a$) for the fcc and bcc structures, respectively. These are so-called Baldereschi mean-value points,[16] which are supposed to give an approximate value of the integral over the Brillouin zone. As one can see, this point may give a reasonable estimate of the energy of the IPM state, provided that the strongest exchange interaction parameters are restricted by the first two coordination shells.

A substantial improvement can be achieved just by adding one more $\mathbf{q}$ point: two Chadi-Cohen points[17] provide a very good convergence of the integral in both cases. As one can see from Table I, in the case of the fcc structure, the average spin-spin correlation functions for the set of the two Chadi-Cohen points are exactly the same as in the case of the 16-atom supercell,[19] with a "quasirandom" distribution of spin-up and

TABLE I. Spin-spin correlation functions for the first 24 coordination shells of the fcc structure obtained using Baldereschi mean-value point (B-1) (Ref. 16) 2 and 10 Chadi and Cohen **q** points (Ref. 17) (CC-2 and CC-10), and 3, 4, and 8 Monkhorst-Pack **q** points (Ref. 18) (MP-3, MP-4, and MP-8). Last column shows the correlation functions of the 16-atom supercell (SC-16).

	$\tilde{\xi}_{lmn}$						
lmn	B-1	CC-2	CC-10	MP-3	MP-4	MP-8	SC-16
110	− 0.001 53	0.0	0.0	0.0	0.0	0.0	0.0
200	0.001 53	0.0	0.0	0.0	0.0	0.0	0.0
211	− 0.182 99	0.0	0.0	0.0	0.0	0.0	0.0
220	− 0.264 92	0.0	0.0	1.0	0.0	0.0	0.0
310	0.184 52	0.0	0.0	0.0	0.0	0.0	0.0
222	0.200 67	0.0	0.0	0.0	0.0	0.0	0.0
321	0.165 51	0.0	0.0	0.0	0.0	0.0	0.0
400	0.059 69	− 1.0	0.0	1.0	0.0	0.0	− 1.0
330	− 0.292 70	0.0	0.0	0.0	1.0	0.0	0.0
411	0.034 82	0.0	0.0	0.0	0.0	0.0	0.0
420	− 0.203 40	0.0	0.0	0.0	0.0	0.0	0.0
233	− 0.149 26	0.0	0.0	0.0	0.0	0.0	0.0
422	0.265 53	0.0	0.0	1.0	0.0	0.0	0.0
431	0.073 68	0.0	0.0	0.0	0.0	0.0	0.0
510	− 0.219 62	0.0	0.0	0.0	0.0	0.0	0.0
521	− 0.089 94	0.0	0.0	0.0	0.0	0.0	0.0
440	− 0.279 64	1.0	0.0	1.0	0.0	1.0	1.0
433	− 0.550 74	0.0	0.0	0.0	0.0	0.0	0.0
530	− 0.036 60	0.0	0.0	0.0	0.0	0.0	0.0
244	0.192 64	0.0	0.0	0.0	0.0	0.0	0.0
600	0.812 64	0.0	0.0	0.0	1.0	0.0	0.0
532	0.255 53	0.0	0.0	0.0	0.0	0.0	0.0
611	− 0.033 68	0.0	0.0	0.0	0.0	0.0	0.0
620	− 0.048 05	0.0	0.0	1.0	0.0	0.0	0.0

-down magnetic moments in the sites. This means that the total energy of a Heisenberg system obtained in the supercell calculations using the 16-atom supercell and in the spin-wave calculations with the two Chadi-Cohen points should be the same.

The fast convergence of the BZ integral with increasing number of **q** points is clearly seen in Tables I and II, where we also show the spin-spin correlation functions for other sets of **q** points, including those generated by Monkhorst-Pack scheme.[18] In the case of the bcc structure, we also include a point $\mathbf{q}_1 = (\frac{1}{3}, \frac{1}{6}, \frac{1}{2})$, which we found to give very close results for the average magnetic moment and total energy of bcc Fe to those obtained with the set of 29 Monkhorst-Pack **q** points (MP-29). From now on, we will refer to this point as Q-1.

D. Magnetic short-range order in paramagnetic state

One of the advantages of the spin-wave method is a possibility to model a magnetic state with specific magnetic short-range order (MSRO). If the needed values of the spin-spin correlation functions $\xi(\mathbf{R})$ are known, the easiest way to determine the weights of the special points providing these $\xi(\mathbf{R})$ is to determine the corresponding Fourier transforms of $\xi(\mathbf{R})$ using Eq. (7) and then use them in the calculations of the total energy [Eq. (8)].

In this case, the weight of special point $\mathbf{q}_i$ is renormalized as $w_i^{\mathrm{MSRO}} = w_i \xi(\mathbf{q}_i)$, where w_i is the weight in the ideal paramagnetic state [for which $\xi(\mathbf{q}_i) = 1$]. One should, however, bear in mind that these relations are exact only when both $\xi(\mathbf{R})$ and $\xi(\mathbf{q})$ are determined for the whole set of **R** and **q** points, respectively. This is impractical and we therefore would like to consider a simple but useful example of the description of the MSRO in bcc Fe above the magnetic phase transition using Monkhorst-Pack special points.

As an example, we calculate the MSRO in the bcc Fe in paramagnetic state using the classical Monte Carlo method[20] with the exchange interaction parameters [see Eq. (1)] obtained in DLM state using the exact muffin-tin orbital method. We have used 11 first strongest interactions in this case.[21] In Fig. 1, we show the spin-spin correlation functions $\xi(\mathbf{R})$ of bcc Fe in the paramagnetic state at three different temperatures: 1100, 1200, and 1800 K (the magnetic phase transition takes place at about 1060 K). The first temperature is just above (∼40 K) the magnetic phase transition, the second one corresponds approximately to the temperature of the structural α-γ phase transition, and the third one to the highest temperature when the bcc structure is still stable (so-called δ phase), before undergoing the melting phase transition.

The spatial decay of the spin-spin correlation functions can be analyzed using the Ornstein-Zernike function $\exp(-\kappa d)/d$, where κ is the inverse correlation length and d is the relative distance (in units of the lattice constant in this particular case).[22] The inverse correlation length determines the scale relevant for the correct description of the MSRO. If this scale is smaller than the shortest distance between the **q** points for a particular set of special points, the latter can not provide an accurate description of the MSRO.

TABLE II. Spin-spin correlation functions for the first 24 coordination shells of the bcc structure obtained using Baldereschi mean-value point (B-1) (Ref. 16), $\mathbf{q}_1$ point (Q-1), 2 and 8 Chadi and Cohen $\mathbf{q}$ points (Ref. 17) (CC-2 and CC-8), and 3, 4, and 8 Monkhorst-Pack $\mathbf{q}$ points (Ref. 18) (MP-3, MP-4, and MP-8). Last column shows the correlation functions of the 16-atom supercell (SC-16).

	ξ_{lmn}							
lmn	B-1	Q-1	CC-2	CC-8	MP-3	MP-4	MP-8	SC-16
111	0.00	0.0	0.0	0.0	0.0	0.0	0.0	0.000
200	0.00	−0.3333	0.0	0.0	0.0	0.0	0.0	0.000
220	−0.25	−0.0833	0.0	0.0	0.0	0.0	0.0	0.000
311	0.00	0.0	0.0	0.0	0.0	0.0	0.0	0.000
222	−0.25	0.25	0.0	0.0	1.0	0.0	0.0	0.000
400	0.00	0.0	−1.0	0.0	1.0	0.0	0.0	−0.333
331	0.00	0.0	0.0	0.0	0.0	0.0	0.0	0.000
420	0.25	0.1667	0.0	0.0	0.0	0.0	0.0	0.000
422	0.25	−0.0833	0.0	0.0	0.0	0.0	0.0	0.000
511	0.00	0.0	0.0	0.0	0.0	0.0	0.0	0.000
333	0.00	0.0	0.0	0.0	0.0	1.0	0.0	0.000
440	−0.25	−0.25	1.0	0.0	1.0	0.0	0.0	−0.333
531	0.00	0.0	0.0	0.0	0.0	0.0	0.0	0.000
442	−0.25	−0.0833	0.0	0.0	0.0	0.0	0.0	0.000
600	−1.00	−0.3333	0.0	0.0	0.0	1.0	0.0	0.000
620	0.00	0.1667	0.0	0.0	0.0	0.0	0.0	0.000
533	0.00	0.0	0.0	0.0	0.0	0.0	0.0	0.000
622	0.25	−0.25	0.0	0.0	1.0	0.0	0.0	0.000
444	0.25	0.25	−1.0	0.0	1.0	0.0	1.0	1.000
711	0.00	0.0	0.0	0.0	0.0	0.0	0.0	0.000
551	0.00	0.0	0.0	0.0	0.0	0.0	0.0	0.000
640	0.00	0.1667	0.0	0.0	0.0	0.0	0.0	0.000
642	−0.25	0.1667	0.0	0.0	0.0	0.0	0.0	0.000
731	0.00	0.0	0.0	0.0	0.0	0.0	0.0	0.000

For instance, $\kappa = 0.23$, 0.656, and 2.487 for the three temperatures: 1100, 1200, and 1800 K, shown in Fig. 1. If we take the Monkhorst-Pack 8-point mesh (MP-8), with the smallest distance between points about 2.22 (in units $1/a$) there is no way to obtain an accurate fit for the MSRO at 1100 K. In this case, the use of a finer grid of $\mathbf{q}$ points is needed. Nevertheless, as one can see in Fig. 1, a small adjustment of the weights of $\mathbf{q}$ points allows one to get quite reasonable spin-spin correlation functions at the first five coordination shells for the MSRO at 1200 K. At the same time, $\xi(\mathbf{q}_i)$ provides a quite accurate description of the MSRO at 1800 K without any adjustment as obvious from Fig. 1.

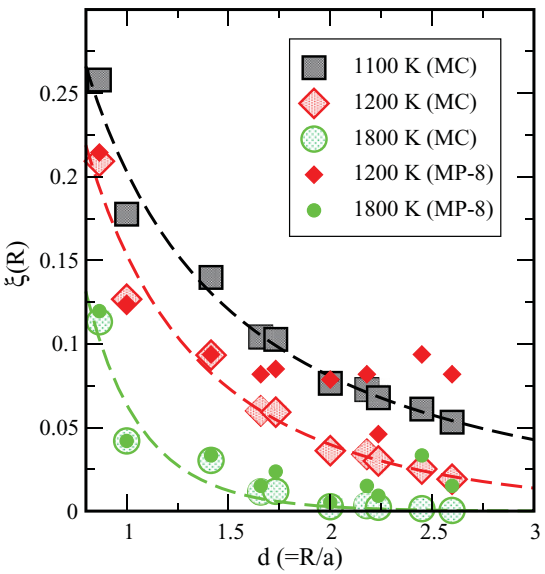

FIG. 1. (Color online) Real-space spin-spin correlation functions in bcc Fe in the paramagnetic state at different temperatures obtained in the Monte Carlo simulations. Fit by Ornstein-Zernike correlation function is shown by dashed line. Small filled symbols are $\xi(\mathbf{R})$ obtained from reweighting the 8-point Monkhorst-Pack grid (MP-8).

Of course, one should bear in mind that the Monkhorst-Pack grid will always produce translationally symmetric $\xi(\mathbf{R})$ since the $\mathbf{q}_i$ points of such a grid are translationally symmetric in the reciprocal space. The translation vectors of $\xi(\mathbf{R})$ are thus just the "reciprocal" vectors of the $\mathbf{q}_i$ mesh. In particular, in the case of MP-8 grid, one of the smallest translation vectors is $\mathbf{T} = (222)$ in units of lattice vector a (or 444 in terms of lmn indices, see Table II), so that $\xi(\mathbf{R} + n\mathbf{T}) = \xi(\mathbf{R})$, and so on. In the presence of the MSRO, additional "harmonics" appear, reducing the range of the repetition of the correlation functions further. However, one can always chose a more dense mesh of $\mathbf{q}$ points if necessary.

III. METHODOLOGY

The electronic-structure calculations have been done by two methods: the exact muffin-tin orbital (EMTO) method[23,24] and projector augmented wave (PAW).[25,26] The EMTO method, being implemented in the Green's function formalism[27] and

combined with the full-charge-density (FCD) technique and CPA,[28] is an accurate tool for doing DLM-CPA total energy calculations. The PAW method as implemented in the Vienna *ab initio* simulation package[29] (VASP) has been used in the calculations of elastic constants, vacancy formation energy, and phonon spectra of bcc Fe in the paramagnetic state.

The EMTO total energies have been calculated using the generalized gradient approximation[30] (GGA) within the full charge density (FCD) formalism. All the self-consistent EMTO-CPA calculations have been performed using an orbital momentum cutoff of $l_{\max} = 3$ for partial waves. The integration over the Brillouin zone has been performed using a $37 \times 37 \times 37$ grid of special **k** points determined according to the Monkhorst-Pack scheme.[18] The core states have been recalculated at each self-consistency iteration.

The PAW calculations have been performed in the GGA.[31] The energy cutoff was set to 450 eV. For all spin-spiral calculations, all the symmetry operations have been switched off. The convergence criterion for the total energy was chosen to be 10^{-5} eV in the lattice parameter calculations and 10^{-8} eV in the elastic constants calculations. The elastic constants have been calculated using a $37 \times 37 \times 37$ grid of special **k** points determined according to the Monkhorst-Pack scheme.[18]

A 27-atom supercell formed by $3 \times 3 \times 3$ translations of a primitive cell of the bcc structure has been used in calculations of vacancy formation energies and forces for the small-displacement method.[32] The small-displacement method in a way similar to that described in Ref. 32 and as implemented in PHON (Refs. 33 and 34) code has been used to calculate the phonon spectrum of paramagnetic iron. The displacement amplitude has been 0.04 Å. The convergence criterion has been chosen to be 10^{-5} eV. The disordered magnetic state calculations have been done using spin-wave approach by averaging the forces that have been obtained by displacements in the $\langle 111 \rangle$ directions for each spin-spiral vector **q**.

Local relaxations have been included in the vacancy formation energy calculations. In order to keep the cubic symmetry of the lattice, which is the case of real macroscopic alloys where it is preserved on average, the form of the unit cells has been kept fixed. At the same time, we have relaxed all the atomic positions in the supercell. The atomic positions were relaxed until the forces on atoms have been less than 10^{-2} eV/Å.

IV. RESULTS AND DISCUSSION

A. Total energy of paramagnetic fcc Co and bcc Fe

In this section, we compare the supercell, DLM-CPA, and spin-wave methods for two systems: fcc Co and bcc Fe. Both are itinerant magnets, which do not satisfy the necessary conditions for Heisenberg systems: Their local magnetic moments and exchange interaction parameters, obtained by a perturbative method, i.e., the magnetic force theorem,[35] depend quite strongly on the global magnetic state.[20,36] In other words, none of these methods is exact for the paramagnetic state of Fe and Co, and therefore this test is merely a comparison of different techniques, and it can not be used to judge the quality of the presentation of the paramagnetic state. The main point here is about efficiency and possibilities.

The electronic-structure and total energy calculations are done by the EMTO method, which can be used in all three cases. In order to avoid systematic errors, all the parameters of the electronic-structure calculations have been exactly the same, but the Monkhorst-Pack grid for the **k**-point integration, which has been reduced in the supercell calculations according to the size of the supercells. In Tables III and IV, we present the results for fcc Co and bcc Fe obtained for the same Wigner-Seitz radius 2.65 a.u.

In the case of Co, however, there are no results for supercell calculations since it has not been possible to get a self-consistently convergent electronic structure for the random magnetic configuration of spin-up and -down Co atoms, the spin-spin correlation functions of which are given in Table I. This is a very good illustration of one of the problems one faces in the supercell modeling of paramagnetic state in the case of itinerant magnets. The origin of the problem can be clearly seen from the results presented in Table III.

Here, we show the energy and (average) magnitude of the local magnetic moments of paramagnetic, ferromagnetic, and antiferromagntic fcc Co. First of all, the antiferromagnetic state of fcc Co with spin-wave vector $\mathbf{q}_{\mathrm{AFM}} = (100)2\pi/a$ is not stable: the magnetic moment vanishes and the system becomes nonmagnetic (last column in Table III). Now, one can notice that the energy of nonmagnetic state is actually very close to that of the DLM state, in spite of the fact that the energy of the ferromagnetic state is an order of magnitude lower. One can also see very large variations of the magnitude of the local magnetic moment. All these point to the weak itinerant nature of magnetism in fcc Co in the paramagnetic state, characterized by a very shallow energy landscape for the magnetic states close to the paramagnetic (and nonmagnetic) one.

It is clear that the spin-wave method allows quite efficient calculations of the paramagnetic state. By using just a single Baldereschi mean-value point, one can obtain a reasonable representation of the paramagnetic state. Obviously, the Chadi-Cohen special points work also quite well. This is also apparently the case of bcc Fe, as one can see in Table IV. Although the variation of the energy of the paramagnetic state is larger in the case of bcc Fe than in the case of fcc Co, it

TABLE III. Total energy and the average magnitude of the local magnetic moment in the "ideal" paramagnetic, FM, and AFM states fcc Co. The total energy is given relative to that in the DLM-CPA model (in mRy).

		IPM							
	DLM-CPA	B-1	CC-2	CC-10	MP-3	MP-8	MP-30	FM	NM (AFM)
ΔE_{tot}	0.0	− 0.35	− 0.54	− 0.51	0.01	− 0.62	− 0.51	− 12.08	1.74
m	1.105	1.170	1.072	1.027	0.209	0.989	1.025	1.667	0.0

TABLE IV. Total energy and the average magnitude of the local magnetic moment in the IPM, FM, and AFM states bcc Fe. The total energy is given relative to that in the DLM-CPA model (in mRy).

	IPM								
	DLM-CPA	B-1	CC-2	CC-8	MP-3	MP-29	sc-16	FM	AFM
ΔE_{tot}	0.0	− 0.81	− 1.43	− 0.59	1.39	− 0.75	0.69	− 13.65	15.45
m	1.956	2.145	2.119	2.100	2.021	2.096	2.095	2.220	1.434

is *relatively* on the same scale, taking into consideration the large variation of the magnetic energy of bcc Fe, which spans about 29 mRy from the AFM to the FM states. It is also clear that there is no such shallow energy landscape in the case of bcc Fe, as in the case of fcc Co.

B. Vacancy formation energy in bcc Fe

Another problem of the supercell approach is the fact that it may require the use of very large model systems or equivalently a large set of smaller systems in the case of defect-formation energy calculations in paramagnetic metals and alloys. The point is that, in this case, it is not sufficient to satisfy Eq. (3) globally, but it should also be valid locally in the vicinity of the defect. This means, for instance, that in the case of a point defect, the local spin-spin correlation functions on the defect site should obey Eq. (3). Besides, in order to have really accurate results, one should also take care of the magnetic structure of atoms surrounding an impurity (vacancy), which should provide on average the necessary spin-spin correlation functions. It is clear that in the end, this is a highly nontrivial problem.

The spin-wave method has an obvious advantage in this case since for a given spin-wave vector, the system is magnetically homogeneous in the sense that all the sites of the lattice are equivalent. Of course, the presence of a defect destroys this equivalence, and moreover, the modeling of a defect requires the use of a finite supercell, which imposes certain boundary conditions. The latter in effect destroys a perfect spin-spiral state with a given wave vector $\mathbf{q}$ unless the translations are multiples of the spin-spiral wavelength. At the same time, it is also clear that the boundary effect can be systematically diminished by increasing the size of the supercell, and the effect of the boundaries is easy to check.

In this work, we have chosen a 27-atom supercell ($3 \times 3 \times 3$) for the vacancy formation energy calculations. Such a supercell provides quite an accurate description of the vacancy formation energy, at least for the purpose of the demonstration of the technique (see, for instance, Ref. 37). Accurate calculations of the vacancy formation energy in real magnetic systems at finite temperature is, in fact, a quite nontrivial task, which is not considered here.

In Table V, we show the vacancy formation energy in bcc Fe in the FM and PM states obtained by the EMTO and PAW methods for the experimental room- and high-temperature (1073 K) lattice constants[38] corresponding to the FM and PM states. The EMTO calculations are less accurate and do not allow us to take local lattice relaxation effects into account, but the EMTO method is used here for comparison of the supercell DLM-CPA and spin-wave results. In the latter case, we have used just a single spin spiral with wave vectors either given by the Baldereschi mean-value point (B-1), or $\mathbf{q}_1$ (Q-1).

It is clear that the spin-wave method yields the results very close to the DLM-CPA calculations. The latter means that cumbersome supercell calculations can be done just by using one mean-value $\mathbf{q}$ point, either Q-1 or B-1. The PAW calculations of unrelaxed vacancy formation energies for MP-8, B-1, and Q-1 also agree well with each other. Unfortunately, we could not stabilize self-consistent calculations with relaxation for single-point sets B-1 and Q-1.

Results presented in Table V allow one to analyze the vacancy formation energy as a function of the magnetic state and lattice parameter and compare it to that obtained in other papers.[39–46] In particular, the effect of the lattice constant on the vacancy formation energy is clearly small in the FM state between 2.84 and 2.90 Å (see also Ref. 39), while it is quite noticeable in the PM state in the same interval. But, the effect of the magnetic state is obviously dominating. The vacancy formation energy in the ideal PM state is about 30% lower than that in the FM state. This reduction is higher than that observed experimentally.[40,41]

Partly, this discrepancy could be due to the MSRO, neglected in the IPM. Using the weights of the MP-8 $\mathbf{q}$-point set for the MSRO at 1800 and 1200 K, we have also determined the effect of the MSRO on the vacancy formation energy (last three columns in the table). As one can see, the MSRO increases the vacancy formation energy by about 7% at 1200 K and brings the theoretical ratio between the FM and PM vacancy formation energy to better agreement with the experimental data. The larger absolute values of the vacancy formation energies can be related to an inaccurate description of the exchange-correlation effects in the GGA.

Finally, we would like to mention the fact that the local relaxations are quite important in both FM and PM states. The relaxation energy in the PM and FM states are -0.23 and -0.21 eV, respectively, for the high-temperature lattice constant, while in the FM state at room temperature it is -0.25 eV, which indicates that the relaxation energy is probably more sensitive to the lattice constant than to the magnetic state.

C. Elastic constants of paramagnetic bcc Fe

The spin-wave method is well suited for the calculation of elastic constants in the absence of the spin-orbit term since, in this case, the spin wave can be oriented arbitrarily with respect to the strain, and thus no average is needed. This is, however, not the case of the supercell approach unless special conditions are satisfied. In particular, the distribution of atoms with the spin-up and -down orientations of magnetic moment should be not only random on average, but it should be homogeneously

TABLE V. Vacancy formation in bcc Fe (in eV) obtained in the FM and PM states at room- (a = 2.86 Å) and high-temperature (a = 2.90 Å) lattice constants (Ref. 38). Other *ab initio* results are obtained in the GGA for the FM state and at the GGA theoretical lattice constant (2.84 Å).

	FM		PM, a = 2.90 (2.84) Å					
	a = 2.86 Å	a = 2.90 Å	DLM	Q-1	B-1	MP-8	MSRO 1800 K	(MP-8) 1200 K
				IPM				
EMTO, unrelaxed	2.61	2.62	2.24 (2.05)	2.26 (2.15)	2.31 (2.17)			
PAW, unrelaxed	2.51	2.53		2.00	1.97	2.00	2.05	2.09
PAW, relaxed	2.26	2.32				1.77	1.84	1.90
			Experimental data					
Ref. 40		2.00				1.79		
Ref. 41		1.60				1.50		
Ref. 42						1.50		
Ref. 43						1.40		
Ref. 44						1.60		
			Other *ab initio* calculations					
FP-LMTO, relaxed (Ref. 37)		2.18						
FP-KKR, unrelaxed (Ref. 39)		2.45						
PAW, relaxed (Ref. 46)		2.14						
PAW, relaxed (Ref. 45)		2.14						

random providing the needed cubic symmetry. The latter can be achieved only for a large-size supercell.

In this work, we have used the EMTO-CPA and PAW method to calculate elastic constants in bcc Fe in the PM state using the same methodology as reported in Ref. 47. However, in order to calculate shear elastic constants using the spin-wave method, one needs to generate a new set of **q** points, which corresponds to a new distorted lattice under the corresponding strain. This leads to a larger number of **q** points due to the reduced symmetry. For instance, in the case of C_{44} and C', the Monkhorst-Pack 8-point set (MP-8) for bcc lattice becomes 18-point sets under the corresponding strains.

The results of the calculations for the bulk modulus B and two shear elastic constants C_{44} and C' are shown in Table VI and compared to the PM results from the other works.[48–50] Again, as in the case of vacancy formation energy, one can see that there is very good agreement between the spin-wave and DLM-CPA calculations. The EMTO results are in fact in quite good agreement with experimental data,[48] at least it is much better than that between the PAW results and experiment. We believe that this is rather accidental since the EMTO method is obviously less accurate in the elastic property calculations than the PAW method. The PAW results should be regarded as the most accurate, and this point indicates an apparent problem. In particular, this concerns C', which is negative in the PAW calculations in the IPM, indicating the mechanical instability of bcc Fe.

The reason for the disagreement between PAW results and experimental data can be related (1) to the fact that our model of the paramagnetic state is oversimplified; (2) to the neglected magnetic short-range-order (MSRO) effects in the paramagnetic state; (3) to the neglected contribution from other type of excitations, vibrational in particular; and (4) to an inaccurate description of the exchange-correlation potential in the GGA. It is also clear that all the above-mentioned approximations can in different ways affect different elastic properties.

For instance, as has been recently demonstrated by Razumovskiy *et al.*,[51] the magnetic state in Fe produces large impact upon C', but has little effect upon the bulk modulus, which exhibits a quite strong volume dependence. Thus, as far as C' concerns, the MSRO should correct the obtained results. This is indeed the case as one can see in Table VI: C' is very sensitive to the MSRO and is positive for the MSRO at 1800 K, which is the point of the liquid-bcc transition. The MSRO at 1200 K is quite strong, and it produces large impact upon C'. Let us note that the calculated value of C' is very close to the experimental data at this temperature.

It is interesting to note that MSRO practically does not affect C_{44} and correct just a little bit the bulk modulus. In fact,

TABLE VI. Bulk modulus B and shear elastic constants C_{44} and C' of Fe in the PM state calculated using EMTO-CPA and PAW methods at the experimental high-temperature lattice parameter, 2.90 Å (Ref. 38). Experimental data (Ref. 48) at 1073 K. Other *ab initio* results: the EMTO-CPA (Ref. 49) and DMFT (Ref. 50) (at T 20% higher the Curie temperature) for a = 2.88 Å.

	EMTO		PAW: IPM	PAW: MSRO (MP-8)		Expt. (1180 K)	DLM	DMFT
	DLM	MP-8	MP-8	1800 K	1200 K	Ref. 48	Ref. 49	Ref. 50
C'	15	10	−5	5	10	13	19	36
C_{44}	104	106	90	90	89	99	129	124
B	121	121	110	112	115	131	132	181[a]

[a]Calculated from the elastic constants reported in Ref. 50.

the electronic correlations should also play an important role according to the recent DMFT calculations by Leonov *et al.*[50] (see Table VI). However, the DMFT results are in much worse agreement for all the elastic properties for some unknown reasons. Apparently, an additional investigation is needed.

D. The phonon spectra of bcc Fe in the paramagnetic state

The final example we would like to demonstrate here is calculations of the phonon spectra in the paramagnetic state. It can be done using different approaches, but here we will use the so-called small-displacement method[32] when the force constants (dynamical matrix) are determined from the Hellman-Feynman forces caused be a small displacement of one atom in the supercell.

First, we start from FM calculations in order to test the convergence of the phonon spectrum with respect of the supercell size. In Fig. 2, we show phonon spectrum of bcc Fe in the FM state obtained in 27- ($3 \times 3 \times 3$) and 64-atom ($4 \times 4 \times 4$) supercell calculations. As one can see, the quantitative agreement with the experiment[52] is obtained only in the case of the 64-atom supercell. Unfortunately, we have not been able to run spin-spiral calculations for 64-atom supercell due to restrictions of computer facilities, and thus results presented below for the 27-atom supercell will be quite in error. Thus, they should be considered as a demonstration of the technique in this particular case.

Being the second derivative of the total energy with respect to displacements, the force constants in the PM state are determined as the average of the force constants for the spin spirals in the set

$$\tilde{\Phi}_{\alpha\beta}(\mathbf{R}) = \sum_i w_i \Phi^i_{\alpha\beta}(\mathbf{R}). \tag{12}$$

Here, $\tilde{\Phi}_{\alpha\beta}(\mathbf{R})$ is the average force constant matrix for lattice vector $\mathbf{R}$; α and β are the x, y, and z indexes; $\Phi^i_{\alpha\beta}(\mathbf{R})$ the force constant matrix for a specific spin-spiral state $\mathbf{q}_i$. Since the spin-spiral state lowers the point group symmetry of the underlying lattice, but, at the same time, $\Phi^i_{\alpha\beta}(\mathbf{R})$ are supposed to preserve this symmetry as it is preserved in the paramagnetic state, $\Phi^i_{\alpha\beta}(\mathbf{R})$ should be determined either by averaging over nonequivalent (with respect to the spin-spiral state) displacements or equivalently over the star of the $\mathbf{q}_i$ vector.

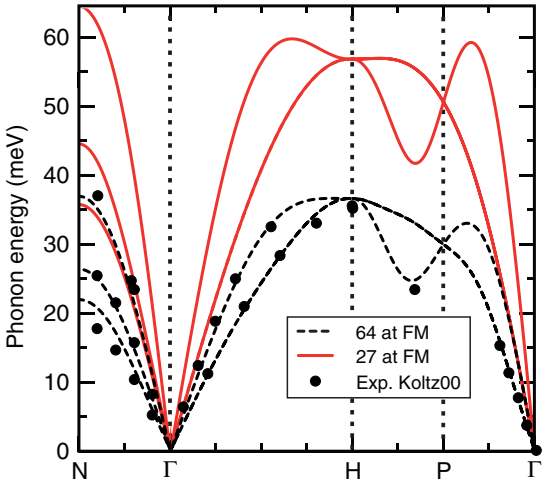

FIG. 2. (Color online) Phonon spectrum of bcc Fe in the FM state from 64- and 27-atom supercell calculations. The experimental data are taken from Ref. 52.

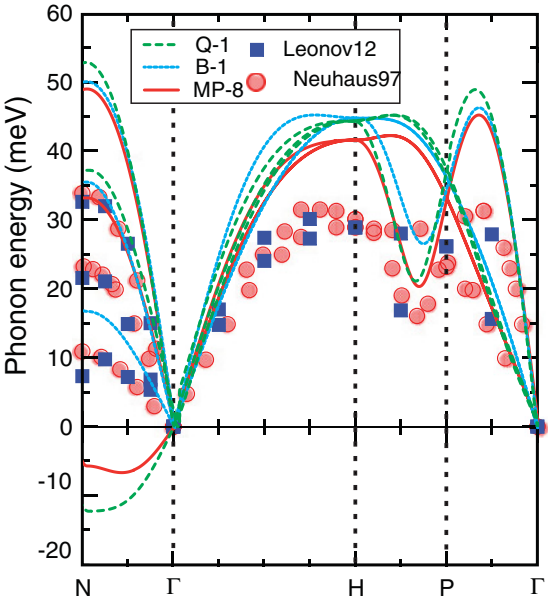

FIG. 3. (Color online) Calculated phonon dispersion of PM iron at 1073 K lattice constant (Ref. 38). Paramagnetic state is calculated using DLM-CPA and spin wave with the selected special mean-value point $\mathbf{q} = (\frac{1}{6}, \frac{1}{3}, \frac{1}{2})$ (Q-1), the Baldereschi mean-value point (B-1), and integration of the magnon spectrum in the corresponding IBZ using eight special points determined according to the Monkhorst-Pack scheme (MP-8). The results are compared with PM DMFT calculations from Ref. 50 and PM experimental data from Ref. 53.

In Fig. 3, we show our results of for PM Fe obtained at the high-temperature lattice constant[38] together with experimental data[53] and recent DMFT results.[50] In our calculations, we have used the 8-point set of the Monkhorst-Pack $\mathbf{q}$ points (MP-8), the Baldereschi mean-value point (B-1), and $\mathbf{q}_1$ point (Q-1). The agreement between all the results obtained by the spin-wave method is good, except the T_1 mode in the $\Gamma-$N direction ($[\xi\xi 0]$), for which the MP-8 and Q-1 spin-wave sets yield negative energy leading to dynamical instability, while B-1 yields positive energy.

Let us note that both DMFT and experimental studies indicate a pronounced softening of the T_1 mode, but, of course, in reality bcc Fe in the PM state is dynamically stable. As in the case of elastic constants, the dynamical instability of bcc Fe in the PM state in the spin-wave calculations is related most probably to the magnetic SRO effects. The additional reason, relevant for Fe in the high-temperature δ phase, can be connected with phonon-phonon interactions or anharmonic effects, which are apparently important close the melting point. Nevertheless, we leave this point to further theoretical investigations.

V. CONCLUSIONS

We have proposed the spin-wave method for the total energy of the paramagnetic state. It is based on the average over the total energies of the planar spin spirals and it is equivalent to the DLM model for Heisenberg systems. As has been demonstrated, it yields results very close to those

obtained by the DLM-CPA approach for fcc Co and bcc Fe. Although it is quite computationally demanding (partly due to inefficiency of the code we have used in the case of the spin-spiral calculations), it provides new opportunities for *ab initio* investigation of metals in the paramagnetic state. In particular, it allows one to calculate the defect-formation energies, elastic constants, and phonon spectrum. Besides, it can be used to take MSRO effects into consideration, which is hardly possible to do by any other *ab initio* technique. Of course, one should bear in mind that the spin-wave method describes accurately only the energetics of the Heisenberg system. This point, however, concerns all the existing techniques, such as the DLM-CPA and supercell approaches.

ACKNOWLEDGMENTS

We wish to thank O. Peil for valuable comments and suggestions and F. Koermann and T. Hickel for the help with VASP input data files for spin-spiral calculations. Computer resources for this study have been provided by the Swedish National Infrastructure for Computing (SNIC) and MATTER Network, at the National Supercomputer Center (NSC), Linköping. This work was performed within the VINNEX center Hero-m, financed by the Swedish Governmental Agency for Innovation Systems (VINNOVA), Swedish industry, and the Royal Institute of Technology (KTH). A.V.R. acknowledges the support of the Swedish Research Council (VR).

*a.v.ruban@gmail.com

[1] A. I. Lichtenstein, M. I. Katsnelson, and G. Kotliar, Phys. Rev. Lett. **87**, 067205 (2001).
[2] M. Cyrot, Phys. Rev. Lett. **25**, 871 (1970); J. Phys. (Paris) **33**, 125 (1972).
[3] J. Hubbard, Phys. Rev. B **19**, 2626 (1979); **20**, 4584 (1979); **23**, 5974 (1981).
[4] H. Hasegawa, J. Phys. Soc. Jpn. **49**, 963 (1980).
[5] B. L. Gyorffy, A. J. Pindor, J. B. Staunton, G. M. Stocks, and H. Winter, J. Phys. F: Met. Phys. **15**, 1337 (1985).
[6] P. Soven, Phys. Rev. **156**, 809 (1967).
[7] B. L. Gyorffy, Phys. Rev. B **5**, 2382 (1972).
[8] P. Söderlind, A. Landa, and B. Sadigh, Phys. Rev. B **66**, 205109 (2002).
[9] P. Söderlind, A. Landa, B. Sadigh, L. Vitos, and A. Ruban, Phys. Rev. B **70**, 144103 (2004).
[10] B. Alling, T. Marten, and I. A. Abrikosov, Phys. Rev. B **82**, 184430 (2010).
[11] L. M. Sandratskii, Adv. Phys. **47**, 91 (1998).
[12] J. Kübler, J. Phys.: Condens. Matter **18**, 9795 (2006).
[13] M. Uhl, L. M. Sandratskii, and J. Kübler, Phys. Rev. B **50**, 291 (1994).
[14] M. Uhl and J. Kübler, Phys. Rev. Lett. **77**, 334 (1996).
[15] In this case, condition (3) is to be satisfied for all coordination shells p where magnetic exchange interactions J_p are not negligible.
[16] A. Baldereschi, Phys. Rev. B **7**, 5212 (1973).
[17] D. J. Chadi and M. L. Cohen, Phys. Rev. B **8**, 5747 (1973).
[18] H. J. Monkhorst and J. D. Pack, Phys. Rev. B **13**, 5188 (1976).
[19] A. V. Ruban, S. I. Simak, S. Shallcross, and H. L. Skriver, Phys. Rev. B **67**, 214302 (2003).
[20] A. V. Ruban, S. Shallcross, S. I. Simak, and H. L. Skriver, Phys. Rev. B **70**, 125115 (2004).
[21] The first 11 interactions (in mRy) used in the MC simulations are $J_{(h,h,h)} = 1.7514$, $J_{(2h,0,0)} = 0.0798$, $J_{(2h,2h,0)} = 0.0680$, $J_{(3h,3h,h)} = 0.0145$, $J_{(2h,2h,2h)} = -0.1552$, $J_{(4h,0,0)} = -0.0278$, $J_{(3h,3h,h)} = -0.0209$, $J_{(4h,2h,0)} = -0.0020$, $J_{(4h,2h,2h)} = -0.0265$, $J_{(3h,3h,3h)} = 0.0821$, $J_{(5h,3h,3h)} = 0.0081$, $J_{(4h,4h4h)} = -0.0063$, where h is half of the lattice constant. The simulation box in the MC simulations was $24 \times 24 \times 24$. Let us note, that it is impossible at the moment to take into consideration the dependence of the exchange interaction parameters on the MSRO.
[22] N. M. Rosengaard and B. Johansson, Phys. Rev. B **55**, 14975 (1997).
[23] O. K. Andersen, O. Jepsen, and G. Krier, in *Methods of Electronic Structure Calculations*, edited by V. Kumar, O. K. Andersen, and A. Mookerjee (World Scientific, Singapore, 1994), pp. 63124.
[24] R. W. Tank and C. Arcangeli, Phys. Status Solidi B **217**, 89 (2000).
[25] P. E. Blöchl, Phys. Rev. B **50**, 17953 (1994).
[26] G. Kresse and D. Joubert, Phys. Rev. B **59**, 1758 (1999).
[27] L. Vitos, *Computational Quantum Mechanics for Materials Engineers* (Springer, London, 2007).
[28] L. Vitos, I. A. Abrikosov, and B. Johansson, Phys. Rev. Lett. **87**, 156401 (2001).
[29] G. Kresse and J. Furthmuller, Phys. Rev. B **54**, 11169 (1996).
[30] J. P. Perdew, K. Burke, and M. Ernzerhof, Phys. Rev. Lett. **77**, 3865 (1996).
[31] J. P. Perdew, J. A. Chevary, S. H. Vosko, K. A. Jackson, M. R. Pederson, D. J. Singh, and C. Fiolhais, Phys. Rev. B **46**, 6671 (1992).
[32] G. Kresse, J. Furthmüller, and J. Hafner, Europhys. Lett. **32**, 729 (1995).
[33] D. Alfe, [http://chianti.geol.ucl.ac.uk/dario].
[34] D. Alfe, Comput. Phys. Commun. **180**, 2622 (2009).
[35] A. Liechtenstein, M. I. Katsnelson, V. P. Antropov, and V. A. Gubanov, J. Magn. Magn. Mater. **67**, 65 (1987).
[36] S. Shallcross, A. E. Kissavos, V. Meded, and A. V. Ruban, Phys. Rev. B **72**, 104437 (2005).
[37] P. Söderlind, L. H. Yang, J. A. Moriarty, and J. M. Wills, Phys. Rev. B **61**, 2579 (2000).
[38] I. Seki and K. Nagata, ISIJ Int. **45**, 1789 (2005).
[39] T. Mizuno, M. Asato, T. Hoshino, and K. Kawakami, J. Magn. Magn. Mater. **226–230**, 386 (2001).
[40] L. de Schepper, D. Segers, G. Knuyt, L. Dorikens-Vanpraet, M. Dorikens, L. Stals, and P. Moser, Phys. Lett. A **95**, 121 (1983).
[41] H.-E. Schaefer, K. Maier, M. Weller, D. Herlach, A. Seeger, and J. Diehl, Scr. Metall. **11**, 803 (1977).
[42] K. Maier, H. Metz, D. Herlach, and H.-E. Schaefer, J. Nucl. Mater. **69-70**, 589 (1978).
[43] S. M. Kim and W. J. L. Buyers, J. Phys. F: Met. Phys. **8**, L103 (1978).
[44] H. Matter, J. Winter, and W. Triftshauser, Appl. Phys. **20**, 135 (1979).
[45] H. Zhou, Y. Liu, C. Duan, S. Jin, Y. Zhang, F. Gao, X. Shu, and G. Lu, J. Appl. Phys. **109**, 113512 (2011).

[46]X. T. Zu, L. Yang, F. Gao, S. M. Peng, H. L. Heinisch, X. G. Long, and R. J. Kurtz, Phys. Rev. B **80**, 054104 (2009).
[47]V. I. Razumovskiy, A. V. Ruban, and P. A. Korzhavyi, Phys. Rev. B **84**, 024106 (2011).
[48]D. J. Dever, J. Appl. Phys. **43**, 3293 (1972).
[49]H. Zhang, B. Johansson, and L. Vitos, Phys. Rev. **84**, 140411 (2011).
[50]I. Leonov, A. I. Poteryaev, V. I. Anisimov, and D. Vollhardt, Phys. Rev. B **85**, 020401 (2012).
[51]V. I. Razumovskiy, A. V. Ruban, and P. A. Korzhavyi, Phys. Rev. Lett. **107**, 205504 (2011).
[52]S. Klotz and M. Braden, Phys. Rev. Lett. **85**, 3209 (2000).
[53]J. Neuhaus, W. Petry, and A. Krimmel, Phys. B (Amsterdam) **234–236**, 897 (1997).